Grid Strength Impedance Metric: An Alternative to SCR for Evaluating System Strength in Converter Dominated Systems

Henderson, Callum; Egea-Alvarez, Agusti; Kneuppel, Thyge; Yang, Guangya; Xu, Lie

Published in:
IEEE Transactions on Power Delivery

Link to article, DOI:
10.1109/TPWRD.2022.3233455

Publication date:
2024

Document Version
Peer reviewed version

Grid Strength Impedance Metric: An Alternative to SCR for Evaluating System Strength in Converter Dominated Systems

Callum Henderson[1], Agusti Egea-Alvarez[1], Thyge Kneuppel[2], Guangya Yang[3], Lie Xu[1]
1 EEE. Dept, PEDEC Group, University of Strathclyde
2 Siemens Gamesa Renewable Energy
3 DTU Wind, PWR Group, Technical University of Denmark
callum.henderson.100@strath.ac.uk

***Abstract*—Short circuit ratio is an outdated measure of system strength in converter dominated systems as the useful behaviour of inverter-based resources is not represented. While still useful for determining fault current provision, converter connected generation contributes to short circuit level and system strength in a different way to traditional synchronous generation. Additionally, traditional measures only account for system strength at the fundamental frequency while converters possess complex interactions across a frequency range. A novel method of determining system strength across this frequency range from the network impedances is proposed in this paper. The approach known as the Grid Strength Impedance Metric, calculates the system strength independently from short circuit level. The unique contribution of grid-following and grid-forming converters is represented by including the multiple-input multiple-output converter output impedances in the calculation. Small-signal impedance models are employed, and the metric is largely concerned with short-term voltage stability, but some inferences can be made for longer timescales. The approach is validated using time domain simulations to check for any identified areas of weakness in the frequency range. The Grid Strength Impedance Metric successfully represents the useful behaviour of grid-forming converters, indicating an enhancement in voltage stiffness in locations of deployment.**

Keywords—Short Circuit Ratio, Grid Stiffness, Converter Impedance, Power System Stability, Grid Forming Converters

I. INTRODUCTION

Electricity networks worldwide are undergoing a paradigm shift as a push for sustainable energy is becoming the new norm [1]. This has been made viable by the introduction of renewable power interfaced by power electronic converters, which are displacing traditional synchronous generators (SG). Inverter based resources (IBR) cover a wide range of sources with a common form of connection to the grid. While necessary to facilitate the introduction of more renewable generation, numerous challenges in terms of performance and stability have been noted [2]. One such issue that has avoided significant attention, especially in the UK, is the reduction of short circuit level (SCL) and system strength.

SCL is the increased current provided during three-phase faults. SGs can provide over-currents (2-4 p.u.) for some minutes during these faults [3]. However, as these machines are removed from the network the onus falls to IBRs. Since converters have strict over-current limits of 1.1-1.2 p.u. the SCL is significantly reduced [4]. In traditional systems with many SGs, the SCL can be expressed as the short-circuit ratio (SCR), the ratio between the current provided during a three-phase fault to the nominal current. Presently, the terms SCL and grid strength are used analogously. The definition of system strength is well defined for traditional networks and links three main aspects: available short-circuit current, susceptibility to voltage disturbances and maximum power transfer. In traditional networks dominated by SGs, the SCL is determined by the physical machine and line impedances. A high SCL is delivered by a low impedance and results in the generator being seen as a stiffer voltage source from the PCC. This increases the resistance to voltage disturbances. A strong network characterised by a high SCR (>3) will have a large volume of short-circuit current, better short-term voltage stability and a larger capability for active power transfer.

When IBRs are considered, the physical network impedances are no longer sufficient to characterise the system [5]. The fault current is now determined by the inverter limit and traditional definitions of SCR are invalid. To avoid this, the most common approach is to ignore the contribution of IBRs from SCR calculations or use an alternative definition [6]. These methods include composite short circuit ratio (CSCR) [7], weighted short circuit ratio (WSCR) [8], short circuit ratio with interaction factors (SCRIF) and equivalent circuit short circuit ratio (ESCR) [9]. Literature surrounding these methods is poorly explained and lacking implementation. The approaches may be correct for determining the available fault current but incorrectly characterize the strength of the network often suggesting reduced voltage stability. Hence, in IBR dominated systems SCL and grid strength should be considered separately [5]. If considered as a single entity, the system can become needlessly strong in terms of voltage disturbances while trying to procure increased fault current and the useful behaviour of converters is not represented. Conversely, representing increased strength as a higher SCL results in 'synthetic' fault current which may be risky to consider [10].

This paper focuses on characterising the voltage support available to the network including IBRs. Traditionally defined weak grids are seen as an issue for grid-following (GFL) converters as the increased network impedance leads to large voltage deviations at the point of common coupling (PCC) and further stability issues related to the phase locked loop (PLL) [11, 12]. Grid-forming (GFM) converters are often proposed as a solution as they increase the system strength in areas where they operate [5]. However, this behaviour has yet to be quantitatively measured. This paper presents a novel method of classifying the system strength using the IBR equivalent impedance of both converter types. The proposed technique, known as the Grid Strength Impedance Metric (GSIM) builds upon traditional methods of SCR but instead considers the contribution of converters to the voltage stability of the network utilising the converter

output impedance. This allows the fast identification of possible issues prior to stability analysis, similar to the way the way SCR is presently used but inclusive of crucial converter actions in quasi-steady state. The ability to represent frequencies other than the fundamental allows for the identification of possible sub-synchronous oscillations (SSO) and harmonic interactions. The metric can showcase the difference in behaviour between GFL and GFM converters. The new method differs from any previous implementations for the following reasons:

1. *Network voltage support is calculated independent of fault current*
2. *IBR are now represented with complex control interactions included utilising MIMO impedances*
3. *The different behaviour of all network components including SGs, GFL and GFM is now represented*
4. *The strength is represented for a frequency range*
5. *The metric can be caluclated for any resource type and topology where an impedance trace can be formed*

GSIM and SCR are synonymous for traditional networks for all frequencies. The scale is equal for both and the same conclusions for low and high SCR networks can be made using GSIM with a more accurate representation of modern components. The frequency dependent behaviour of GSIM is simpler to understand than Bode or Nyquist techniques. Moreover, GSIM shows significant promise in allowing more IBRs to be added to the network, even in networks conditions that would previously be considered unsuitable using SCR. The approach uses frequency sweeps to determine the output impedance or admittance and therefore forms a black box approach where previous knowledge of the converter control structure is not required.

II. Alternative SCR Definitions

Several new stability indices based on SCR for networks with a high penetration of IBRs have been proposed [7, 9, 13]. Simpler indices look at the contribution of fault current and use this to infer information about the voltage stability, interactions, and grid stiffness.

A. Composite Short Circuit Ratio

Initially proposed by GE, CSCR calculates the grid strength considering all electrically close converters [7]. All converters of interest are assumed to be connected to a single bus and the strength is calculated including power contributions from converters but without fault current contribution:

$$CSCR = \frac{CSC_{MVA}}{MW_{VER}} \tag{1}$$

Where CSC_{MVA} is the fault level contribution excluding converters and MW_{VER} is the sum of nominal power ratings of the connected converters.

B. Weighted Short Circuit Ratio

WSCR has been most notably applied in defining operational limits in Texas [13]. The approach is similar to CSCR but now analyses key points on the network by considering multiple buses:

$$WSCR = \frac{\Sigma_i^N SCMVA_i \times P_{RMW_i}}{\left(\Sigma_i^N P_{RNW_i}\right)^2} \tag{2}$$

Where $SCMVA_i$ is the short circuit capacity at bus i and P_{RMW_i} is the rated power output of the ith converter.

C. Short circuit ratio with interaction factors

The short circuit ratio with interaction factors (SCRIF) looks to augment previous definitions of SCR with a component that captures voltage deviations. This voltage sensitivity is captured via an interaction factor:

$$IF_{ij} = \frac{\Delta V_i}{\Delta V_j} \tag{3}$$

The SCRIF is then determined:

$$SCRIF_i = \frac{S_i}{P_i + \Sigma_j\left(IF_{ij} \times P_j\right)} \tag{4}$$

Subscript j represents all electrically close converters or buses. IF_{ij} is the interaction factor of bus j on bus i, ΔV_i and ΔV_j are the voltage deviations at the ith and jth bus, respectively, S_i and P_i are the fault level contribution and nominal power rating at bus i and P_j is the nominal power at bus j. This suggests that a stiff voltage source inserted at bus i, would decrease the interaction factor, raise the SCRIF and bus i would become more stable. Converters are considered here in terms of power and line impedance, but the control action represented by the equivalent impedance appears to be disregarded preventing dissemination between GFL and GFM devices. It is challenging to determine exactly how the converter is represented in literature surrounding SCRIF as the calculation of the voltage disturbances for the IF is not well described. Approaches looking at the steady state reaction to disturbance injection at the fundamental frequency likely do not accurately represent the converter action in quasi-steady state conditions.

D. Equivelent Short Circuit Ratio

The ESCR is very similar to the traditional SCR, but now considers all physical impedances on the network:

$$ESCR = \frac{1}{Z_{sys,PU}} = Y_{sys,PU} \tag{5}$$

Where $Z_{sys,PU}$ and $Y_{sys,PU}$ are the system impedance and admittance, respectively. The ESCR is not necessarily novel, it is the traditional SCR determined at a different point on the network, closer to the device of interest. The metric suggests the maximum network impedance that the converter can operate under. However, the impedance due to converter control is not considered. This method forms the basis for the novel approach proposed in this paper utilizing converter admittance models to extract an equivalent rating of strength.

E. Drawbacks of present methods

The drawbacks of the previous methods include: the inability to differentiate between GFL and GFM devices, only representing strength at the fundamental frequency (FF) and continuing to describe the network as if it was dominated by SGs. For example, CSCR and WSCR cannot represent

different types of converter behaviour as they consider the power contribution which is the same for both GFL and GFM. ESCR only considers the physical line impedances of the converters which is again not dependent on converter type. SCRIF begins to study interactions however, it is only described at the FF where the true behaviour of the converters is challenging to represent using conventional measurement techniques such as IF. Additionally, the IF is based on physical impedances and does not include any converter control components. Hence, the SCRIF will underestimate the strength of the network when GFM converters are included.

All methods continue to couple voltage stiffness and fault current into one metric which is not valid for the modern system. The behaviour of converters during faults is vastly different from the quasi-steady state behaviour and therefore characterising the normal operating behaviour via the fault characteristic is futile. The voltage strength provided by converters must be calculated considering the behaviour of the converter in the quasi-steady state which is achievable by utilising the equivalent converter output impedance. When considering quasi-steady state conditions, increased voltage stability from IBRs can occur without increased fault current with appropriate control.

III. Converter Impedance

In this section two types of control structure are presented: a standard current control based GFL algorithm with PLL, and a simplified virtual synchronous machine (VSM) structure representing a GFM controller. Each control structure is presented with key components discussed. The level of control detail used is applicable when considering systems with only a few converters connected. However, aggregation techniques are likely required if studying the wider system.

A. Impedance formulation

A state-space model is created to facilitate the generation of the converter admittance:

$$\Delta\dot{\boldsymbol{x}} = \Delta\boldsymbol{A}\boldsymbol{x} + \Delta\boldsymbol{B}\boldsymbol{u} \tag{6}$$

$$\Delta\boldsymbol{y} = \Delta\boldsymbol{C}\boldsymbol{x} + \Delta\boldsymbol{D}\boldsymbol{u} \tag{7}$$

Where $\boldsymbol{x}$, $\boldsymbol{u}$ and $\boldsymbol{y}$ are the model state, input and output vectors respectively, and $\boldsymbol{A}, \boldsymbol{B}, \boldsymbol{C}$ and $\boldsymbol{D}$ are the state, input, output and feedthrough matrices respectively. Once the model is linearised the converter admittance is classified as the ratio of the response current from the converter ($\boldsymbol{I_c}$) to the voltage disturbance at the PCC ($\boldsymbol{U_{PCC}}$):

$$\boldsymbol{Y}_c = \frac{\Delta\boldsymbol{I}_c}{\Delta\boldsymbol{U}_{PCC}} \tag{8}$$

The converter admittance is determined by the physical filter components and the control architecture. The capacitor between the RL filter and the PCC is not included but can be modelled as a load effect. To generate the admittance from the state-space matrix the model inputs and outputs are selected to be:

$$\boldsymbol{u} = \begin{bmatrix} \Delta\boldsymbol{u}_{q,PCC} \\ \Delta\boldsymbol{u}_{d,PCC} \end{bmatrix} \tag{9}$$

$$\boldsymbol{y} = \begin{bmatrix} \Delta\boldsymbol{i}_{q,c} \\ \Delta\boldsymbol{i}_{dc,} \end{bmatrix} \tag{10}$$

The state-space then represents the converter admittance:

$$\begin{bmatrix} Y_{qq,c} & Y_{qd,c} \\ Y_{dq,c} & Y_{dd,c} \end{bmatrix} = \frac{\boldsymbol{y}}{\boldsymbol{u}} = \frac{\Delta\boldsymbol{i}}{\Delta\boldsymbol{u}} \tag{11}$$

The impedances are modelled in the synchronous reference frame to ensure all interactions can be accounted for and easily modelled.

B. Grid-following

A control diagram of the GFL structure which has been widely applied in literature is provided in Fig. 1 [14-16]. An in-depth description of the control structure and tuning recommendations can be found in [17]. However, a short summary is provided in this section. Synchronisation is provided via a PLL and the current flow through the filter impedance is regulated in the synchronous reference frame via two PI controllers with appropriate cross-coupling terms and voltage feedforwards. A current limiting algorithm is not included as the non-linear behaviour cannot be represented in small-signal models and separating quasi-steady state from fault behaviour is a main motivation of this work. Two outer loop PI controllers regulate active power on the q-axis and PCC voltage on the d-axis. This is due to the q-axis voltage being synchronised with the a-phase voltage.

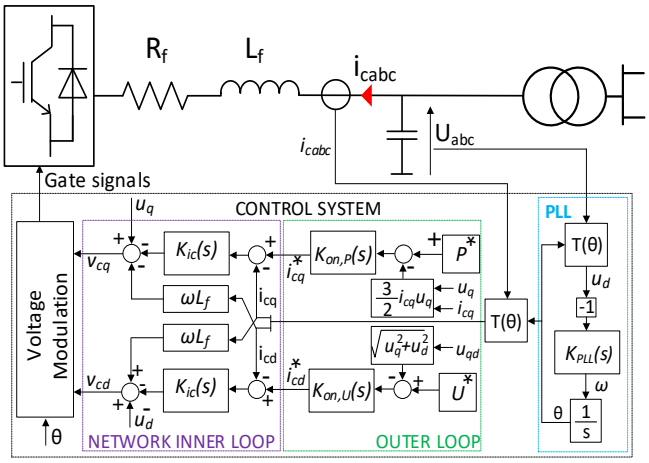

Fig. 1. Grid-following controller structure

C. Grid-forming

A simplified VSM structure without internal current control (CC) is used in this work. This work is concerned with short-term voltage stability and not with fault ride through (FRT). Therefore, internal CC is avoided as it raises the converter output impedance and reduces the effectiveness of the GFM structure [5]. Furthermore, structures excluding internal CC have been gaining interest in recent literature [15, 18-20]. Ongoing work is looking at FRT of VSM controllers without CC and therefore the structures are of importance [21]. A full description can be found in [17, 21] but is summarised here. Synchronisation with the network is provided via an active power PI controller representing the power swing equation. A PI directly regulates the PCC voltage via the q-axis. Park transforms are not utilised as the active power and PCC voltage magnitude can be calculated

in the stationary frame. An inverse park transform is used to translate the synchronous frame voltage commands to abc.

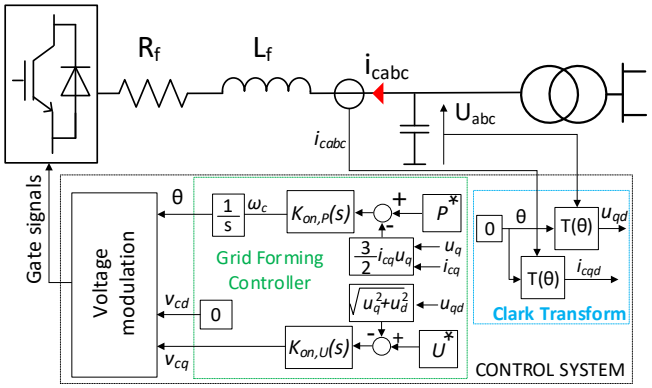

Fig. 2. Grid-forming controller structure

IV. Grid Strength Impedance Metric

Using the defined impedance models the grid strength impedance metric (GSIM) for classifying network strength can be postulated. This is achieved by using the admittance models discussed that describe the performance of the converter in quasi-steady state. This normal operating behaviour is vastly different from fault conditions and allows the decoupling of voltage strength from fault current provision. However, the admittances and hence GSIM are operating point dependent and a range of cases should be studied. Additionally, the poor accuracy of some small-signal models at high frequencies should be considered [22].

A. Defining GSIM

Firstly, the base impedance of the network must be specified using the conventional method:

$$Z_b = \frac{V_b^2}{S_b} \tag{12}$$

Where Z_b, V_b and S_b are the base impedance, voltage and power, respectively. The base impedance can then be used to determine the resistance and inductance parameters for a Thevenin equivalent base grid:

$$R_b = Z_b \frac{R}{X} \tag{13}$$

$$L_b = \frac{Z_b}{\omega_g} \tag{14}$$

$$\boldsymbol{Z}_b = \begin{bmatrix} R_b + sL_b & \omega_b L_b \\ -\omega_b L_b & R_b + sL_b \end{bmatrix} \tag{15}$$

Where $\boldsymbol{Z}_b$ is the base impedance expressed in the synchronous reference frame, ω_b is the FF, R_b and L_b are the base resistance and inductance, respectively and R/X is the desired ratio of resistance to reactance of the network. The system admittance Y_{sys} contains all components of the network under study including a Thevenin equivalent grid with SCR applied and any connected inverter-based resources. Since the impedance/admittance matrices form MIMO systems, the eigenloci of the impedance/admittance matrices across the frequency range are considered. This is a common approach in impedance-based stability methods [23-30]. The impedance/admittance for the base or converter can be obtained from a frequency scan of the physical network which makes GSIM applicable in black box scenarios [31]. Alternatively, a frequency response of a state-space model similar to (11) or transfer function model similar to (15) can be utilised:

$$\boldsymbol{Y}_{sys}(s) = \begin{bmatrix} Y_{qq}(s) & Y_{qd}(s) \\ Y_{dq}(s) & Y_{dd}(s) \end{bmatrix} \tag{16}$$

$$\boldsymbol{Z}_b(s) = \begin{bmatrix} Z_{qq}(s) & Z_{qd}(s) \\ Z_{dq}(s) & Z_{dd}(s) \end{bmatrix} \tag{17}$$

Where $\boldsymbol{Y}_{sys}(s)$ is the 2x2 MIMO transfer function matrix describing the selected system admittance and $\boldsymbol{Z}_b(s)$ is the 2x2 MIMO transfer function matrix describing the base impedance. Each of the 2x2 matrices then produces two eigenloci denoted q and d:

$$\lambda\left(\boldsymbol{Y}_{sys}(s)\right) = \begin{bmatrix} \left|\lambda_{Y_{sys,q}(s)}\right| \\ \left|\lambda_{Y_{sys,d(s)}}\right| \end{bmatrix} \tag{18}$$

$$\lambda\left(\boldsymbol{Z}_b(s)\right) = \begin{bmatrix} \left|\lambda_{Z_{b,q}(s)}\right| \\ \left|\lambda_{Z_{b,d}(s)}\right| \end{bmatrix} \tag{19}$$

Where $\lambda\left(\mathbf{Y}_{sys}(s)\right)$ and $\lambda\left(\mathbf{Z}_b(s)\right)$ are the eigenloci of the system admittance and base impedance, respectively. These eigenvalues represent the magnitude of impedance or admittance in the synchronous reference frame. GSIM is then obtained via the elementwise multiplication (denoted $\odot$) of (18) and (19) which forms an impedance ratio:

$$\begin{bmatrix} GSIM_q(s) \\ GSIM_d(s) \end{bmatrix} = \lambda(\boldsymbol{Y}_{sys}(s)) \odot \lambda(\boldsymbol{Z}_b(s)) \tag{20}$$

Where $GSIM_q(s)$ and $GSIM_d(s)$ are the q and d axis GSIM components, respectively. These components act in unison with interaction between axes to affect the stability of the grid. Therefore, the final GSIM definition combines these values into a single metric relating to the PCC voltage magnitude:

$$GSIM(s) = \sqrt{\frac{GSIM_q(s)^2 + GSIM_d(s)^2}{2}} \tag{21}$$

The converter will have a vastly different impedance during faults compared to normal operation and GSIM is not representative of fault behaviour by design.

B. Exploring the Properties of GSIM

Since system strength is normally obtained at the FF, the 0 Hz component in the synchronous reference frame can be extracted for initial study. If the traditional network is analysed without converters GSIM is equal to the SCR. This can be proven if a base impedance is generated for a 3 MW grid at 690 V with an X/R of 10 and FF of 50 Hz. This gives an example base impedance, resistance and inductance of 159 mΩ, 15.9 mΩ and 505 μH, respectively. If the system impedance is then considered as a Thevenin equivalent network with an SCR of 3 applied then an example system impedance, resistance and inductance of 53 mΩ, 5.3 mΩ and

This article has been accepted for publication in IEEE Transactions on Power Delivery. This is the author's version which has not been fully edited and content may change prior to final publication. Citation information: DOI 10.1109/TPWRD.2022.3233455

170 µH, respectively. Constructing the 2x2 base impedance and system impedances using the form described (15):

$$\boldsymbol{Z}_{b,e} = \begin{bmatrix} 0.0159 + s0.505x10^{-3} & 0.159 \\ -0.159 & 0.0159 + s0.505x10^{-3} \end{bmatrix} \quad (22)$$

$$\boldsymbol{Z}_{sys,e} = \begin{bmatrix} 0.0053 + s0.17x10^{-3} & 0.053 \\ -0.053 & 0.0053 + s0.17x10^{-3} \end{bmatrix} \quad (23)$$

Where $\boldsymbol{Z}_{b,e}$ is the example base impedance matrix and $\boldsymbol{Z}_{sys,e}$ is the example system impedance matrix. The frequency response of each impedance can be generated and the eigenvalues extracted for the FF component:

$$\left|\lambda\left(\boldsymbol{Z}_{b,e}(0\ Hz)\right)\right| = \begin{bmatrix} 0.1598 \\ 0.1598 \end{bmatrix} \quad (24)$$

$$\left|\lambda\left(\boldsymbol{Z}_{sys,e}(0\ Hz)\right)\right| = \begin{bmatrix} 0.0532 \\ 0.0532 \end{bmatrix} \quad (25)$$

Where $\lambda\left(\mathbf{Z}_{b,e}(0\text{ Hz})\right)$ and $\lambda\left(\mathbf{Z}_{sys,e}(0\text{ Hz})\right)$ are the eigenvalues of the frequency response of the base and system impedances, respectively at the FF. The magnitude of the eigenvalues in each case is equal to the magnitude of the impedance of each of the base and system impedances. If the GSIM is calculated dividing by $Z_{sys,e}$ instead of multiplying by the admittance for simplicity, the original SCR of 3 is obtained. The process appears somewhat trivial when RL networks are considered but the addition of converters with complex MIMO admittances begins to provide interesting results that are provided in Section V.

GSIM is mathematically equivalent to SCR as it represents the ratio of base impedance to system impedance. If the per-unit impedance form of SCR is described:

$$SCR = \frac{1}{Z_{sys,pu}} \quad (26)$$

Multiplication of both numerator and denominator by the base impedance provides a similar form to GSIM since the eigenloci represent the magnitude of the impedance or admittance. If the FF components are considered then both are equivalent:

$$SCR = \frac{Z_b}{Z_{sys}} \equiv GSIM(0\ Hz) \quad (27)$$

GSIM will have the same implications in terms of voltage stability to traditional SCR definitions. However, the effect of IBRs can now be represented in quasi-steady state. Moreover, the GSIM provides the same value across the frequency range for SG dominated networks. This proves the similarity and provides an initial validation of the method. However, when converters are included, the GSIM varies significantly across the frequency range and shows areas of large/small impedance previously not present on the traditional network at the FF. Since all network components are now fully represented, this should lead to discovery of components interacting to produce SSO and harmonic interactions which are becoming more prevalent in the modern network [32, 33]. Fast identification of these areas of concern is a key benefit of using GSIM to screen stability issues over conventional metrics where they would be overlooked. This is increasingly important for impedance-based stability techniques which require multiple system 'views' from different points for complete analysis. GSIM facilitates fast screening of these problematic points. In the synchronous reference frame, the (0 - 50 Hz) abc components are not directly visible as they would appear (-50 - 0 Hz). However, like most FFTs the impedances are symmetrical around 0 Hz and the 0-50 Hz abc should be reflected accordingly [34]. This may vary when negative sequence components are added but can be address by representing the components in a different reference frame such as the modified sequence domain [35].

V. Network Analysis

Using the developed method, an investigation of different control structures on the GSIM can be considered. Note that GSIM is applicable to any control structure and the two selected for study in this work are representative of some common controller families. A new converter to be connected to the network requires information about the strength of the point it is connecting to. This is completed by considering a new system impedance for the network that is the parallel combination of the original Thevenin equivalent and any converters. The GSIM can then be used to quantify the strength of the node for further connections 'looking' into the PCC. A system is defined to investigate this containing one GFL and one GFM connected to the network. A diagram in provided in Fig. 3 with system parameters shown in Table I.

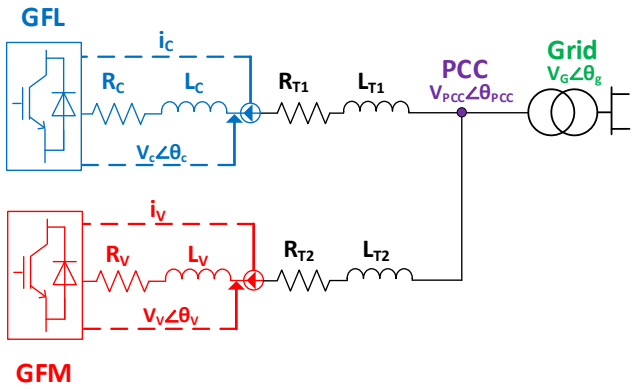

Fig. 3. Multi-converter network topology

Any impedance-based method requires all components to be expressed in a single reference frame. The reference frames on the network can be related to each other via a rotation of which details can be found in [15].

Each converter and filter impedance is combined in series with the respective transmission line (TL) impedance and rotated into the global reference frame. The GFM admittance combination is denoted Y_{VT} and the GFL as Y_{CT}. The strength of the network is analysed by constructing the equivalent circuit from the point of view (PoV) of a converter 'looking' into the PCC. Two PoVs are considered. Firstly, the GFM looking into the network consisting of the grid and the GFL. Secondly, the GFL looking into the network consisting of the grid and GFM. An illustration of this is provided in Fig. 4. The system is simplified for initial analysis but any system topology should be possible providing the impedance traces can be obtained; this may require some topology reduction if the individual MIMO port impedances were to be used, which

is a common approach in impedance-based methods [25, 26]. Failing this, a frequency sweep can be conducted at the bus in question to obtain the combined impedance of the network.

Table I Parameter Table

Parameter	Symbol	Value
Grid Voltage ($V_{L-L,RMS}$)	V_G	690 V
Converter Power	P_C	3 MW
Grid Frequency	ω_G	50 Hz
Base Impedance	$R_b + jX_b$	0.79+j79.4 $m\Omega$
TL1, TL2 Impedance	$R_T + jX_T$	3+j2.8 $m\Omega$
$\text{Filter}_{\text{PVCCN}}$ Impedance	$R_c + jX_c$	1.6+j16 $m\Omega$
$\text{Filter}_{\text{VSM}}$ Impedance	$R_v + jX_v$	1.6+j16 $m\Omega$
PVCCN Controller		
Current Cont. PI Gains	$\text{Kp}_{\text{ic}}, \text{Ki}_{\text{ic}}$	0.15, 1.587
Voltage Cont. PI Gains	$\text{Kp}_{\text{vc}}, \text{Ki}_{\text{vc}}$	1, 10
Power Cont. PI Gains	$\text{Kp}_{\text{pc}}, \text{Ki}_{\text{pc}}$	$1x10^{-6}$, 0.001
PLL PI Gains	$\text{Kp}_{\text{PLL}}, \text{Ki}_{\text{PLL}}$	0.788, 175
VSM Controller		
Power Cont. PI Gains	$\text{Kp}_{\text{pv}}, \text{Ki}_{\text{pv}}$	$5x10^{-7}, 1x10^{-6}$
Voltage Cont. PI Gains	$\text{Kp}_{\text{vv}}, \text{Ki}_{\text{vv}}$	2, 10

Each admittance is modelled as a standalone component and therefore the relationship between voltage and current at the terminals is likely different than when grid connected. The full converter behaviour will not be seen at the PCC and will be scaled by some factor. These factors are determined by considering the system as a combination of Thevenin voltage sources and considering the contribution of voltage to the PCC. A Norton equivalent is also possible. A scaling factor for each source is determined using the physical impedance magnitude seen at the FF:

$$C_{scale} = \frac{Z_g}{Z_{CT} + Z_g} \tag{28}$$

$$V_{scale} = \frac{Z_g}{Z_{VT} + Z_g} \tag{29}$$

$$GV_{scale} = \frac{Z_{VT}}{Z_{VT} + Z_g} \tag{30}$$

$$GC_{scale} = \frac{Z_{CT}}{Z_{CT} + Z_g} \tag{31}$$

Where C_{scale} and V_{scale} are the GFL and GFM scaling factors, respectively and GV_{scale} and GC_{scale} are the network scaling factors for the network when the GFM or GFL converter is connected, respectively. If scaling factors are disregarded the ratings of system strength can significantly over or underestimate the network strength depending on the converter of concern. From Fig. 4 (a), the GFM converter 'sees' a combination of the grid and the GFL converter with related line impedances. The stiffness at the PCC is determined by the system impedance which is the parallel combination of the grid and GFL with scaling applied:

$$\boldsymbol{Y}_{sys1} = C_{scale}\boldsymbol{Y}_{CT} + GC_{scale}\boldsymbol{Y}_g \tag{32}$$

From Fig. 4 (b), the GFL converter 'sees' a combination of the grid and the GFM converter. The stiffness at the PCC is again determined by this system impedance which is now the parallel combination of the grid and GFM impedances:

$$\boldsymbol{Y}_{sys2} = V_{scale}\boldsymbol{Y}_{VT} + GV_{\boldsymbol{scale}}\boldsymbol{Y}_g \tag{33}$$

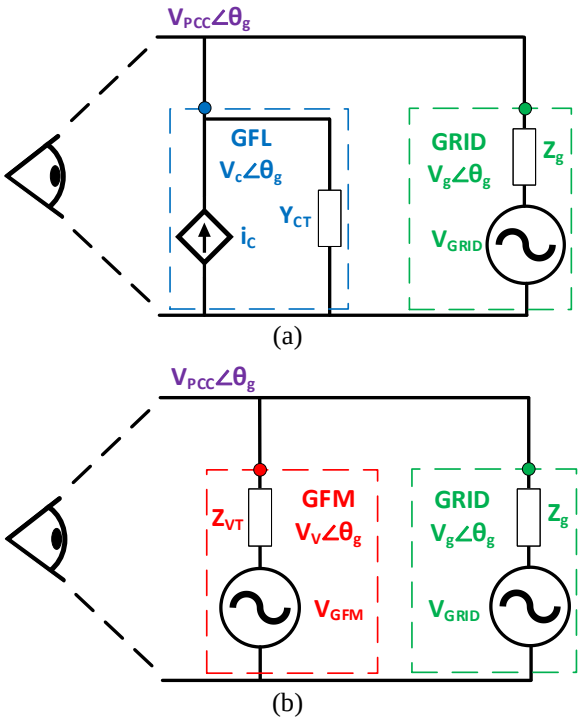

Fig. 4. How the connecting converter views the network: (a) GFM's view (b) GFL's view

The application of each scaling factor allows GSIM to match the rating scale of traditional versions of SCR. Using these two parallel combinations, the effect that GFL control has on system strength can be explored using Y_{sys1} and the GFM control using Y_{sys2}. A final combination of all three components is also defined, with similar scaling terms applied to the voltage sources. However, the scaling factors now become a balance between the converter of concern and the combination of the remaining impedances on the network:

$$s_n = \frac{Z_{p,n}}{Z_n + Z_{p,n}} \tag{34}$$

Where s_n is the scaling factor for the nth component and $Z_{p,n}$ is the combination of all other system impedances excluding the nth component. The third system with scaling applied is:

$$\boldsymbol{Y}_{sys3} = s_1\boldsymbol{Y}_g + s_2\boldsymbol{Y}_{VT} + s_3\boldsymbol{Y}_{CT} \tag{35}$$

The structure of the converter looking into the network is not important, but the power rating should be considered. The base impedance is constant for both systems. Three GSIMs are defined for analysis with a single value obtained via (21):

$$GSIM_{GFL} = \left|\lambda(\boldsymbol{Y}_{sys1}(s))\lambda(\boldsymbol{Z}_{b,3}(s))\right| \tag{36}$$

$$GSIM_{GFM} = \left|\lambda(\boldsymbol{Y}_{sys2}(s))\lambda(\boldsymbol{Z}_{b,3}(s))\right| \tag{37}$$

$$GSIM_{FULL} = \left|\lambda(\boldsymbol{Y}_{sys3}(s))\lambda(\boldsymbol{Z}_{b,6}(s))\right| \tag{38}$$

This article has been accepted for publication in IEEE Transactions on Power Delivery. This is the author's version which has not been fully edited and content may change prior to final publication. Citation information: DOI 10.1109/TPWRD.2022.3233455

The subscript number (3 or 6) in the base impedances $Z_{b,3}(s)$ and $Z_{b,6}(s)$ dictates the base power in MW used for creating the network. The GSIM is used to analyse the effect of each converter type on the voltage stiffness for a weak Thevenin grid (SCR = 1) and a stronger Thevenin grid (SCR = 3). The results showing the scaled GSIM are then compared to alternative SCR methods at the FF in Table II. The SCR shown shows the strength of the initial Thevenin network before the addition of converters. Note the initial Thevenin grid denoted Y_{sys} from Section A is included to validate that the method is synonymous with other definitions in traditional networks.

Table II Comparison of grid-strength metrics

System	SCR	CSCR	ESCR	GSIM
Network (Y_{sys})	1	1	1	1
	3	3	3	3
GFL (Y_{sys1})	2	1.93	1.93	1.65
	6	5.42	5.42	5.61
GFM (Y_{sys2})	2	1.93	1.93	4.42
	6	5.42	5.42	7.17
Full (Y_{sys3})	1	0.95	0.97	1.98
	3	2.85	2.78	3.4

From Table II, all the grid-strength metrics are equal for the standard network with no IBRs. Note that all methods become twice as large when considering only one converter. The grid impedance is designed considering both converters, when one is disregarded, the resultant system becomes twice as strong. The CSCR and ESCR methods are equal when considering one converter only. The CSCR and ESCR underestimate the strength of the network for GFM. Moreover, the control action of the GFL is not properly accounted for with the discrepancy being larger for weaker networks. The GSIM clearly indicates an improvement in voltage strength when GFM converters are added to the system. The value at the FF is conventionally used to infer the strength across the frequency range. This is acceptable as for traditional systems as every impedance component forms an RL system. If it is assumed that the X/R is large, the frequency response of each system is dominated by the inductance. Therefore, the response shape will be similar in all cases with the difference being a scalar multiplier determined by the magnitude of reactance. When converters are introduced, the RL property of the network is reduced. In this case, the GSIM (or traditional SCR) provided at the FF may not cover all the system issues. The value can still be used however, it is probable the FF GSIM will be larger than the actual limit. For example, a GSIM of 1.1 at the FF may only be required to ensure the minimum GSIM at another frequency remains above a lower threshold. Hence, network strength should be considered across the frequency range and GSIM is the only metric at present capable of this.

The GSIM is plotted for the three systems against a range of frequencies in Fig. 5 to showcase the significant variation in system strength with frequency. Additionally, the effect of the GFL PLL bandwidth and GFM voltage control proportional (Kp) and integral (Ki) gain terms are explored. No high frequency components are modelled therefore, a frequency range of 0-400 Hz is sufficient for analysis. The GSIM is provided in the synchronous reference frame where 0 Hz is the FF.

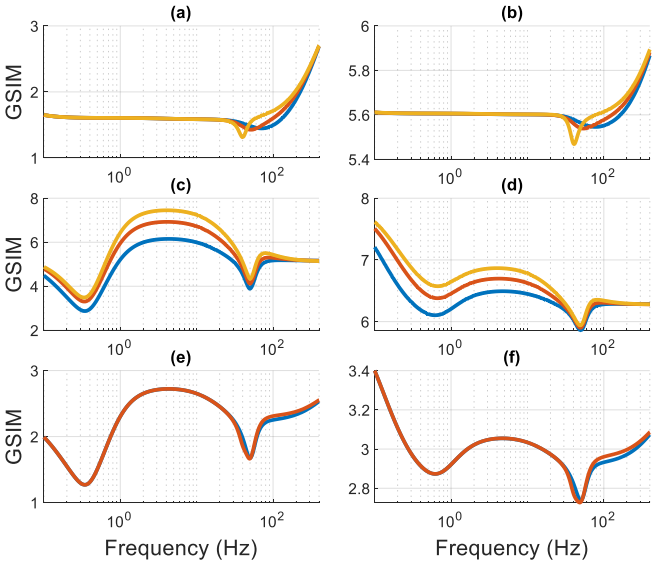

Fig. 5. GSIM for configurations: (a) Y_{sys1} - SCR 1 (b) Y_{sys1} −SCR 3 (c) Y_{sys2} -SCR 1 (d) Y_{sys2} -SCR 3 (e) Y_{sys3} -SCR 1 (f) Y_{sys3} −SCR 3.

Legend. (a)(b) PLL bandwidth: 600 Hz (blue), 500 Hz (orange), 400 Hz (yellow). (c)(d) Voltage Controller Tuning: Kp = 1, Ki = 5 (blue), Kp = 2, Ki = 8 (orange), Kp = 3, Ki = 10 (yellow). (e)(f) PLL Bandwidth: 600 Hz (blue), 400 Hz (orange)

From Fig. 5 (a)(b), the GFL reduces the GSIM below the initial SCR at the FF and up to around 20 Hz. For both SCRs, the GSIM then falls indicating a region of high impedance and poor damping which can be seen to be sensitive to the PLL bandwidth. In Fig. 5 (c)(d), the GFM improves the network strength across most of the frequency range. For both SCRs, the impedance is smaller close to 0 Hz due to the direct voltage control of the GFM and provides a greater strength rating near the FF. This can be increased with faster tunings as shown in Fig. 5 (c)(d). A similar peak can be formed for the GFL traces if the GFL voltage controller is tuned faster but this may harm strength at higher frequencies. This effect is again visible in Fig. 5 (e)(f) around 0 Hz. When the SCR is 1 the GFM converter does more work in supporting the PCC voltage as the GFM scaling factor is larger than the network factor. The PLL bandwidth effects the GSIM over the same range of frequencies as with y_{sys1} but the magnitude is reduced likely due to the increased support from the GFM. When a GFL converter is present GSIM increases at high frequencies due to the system impedance including the converter growing at a slower rate with respect to frequency than the base impedance.

VI. VALIDATION

A validation of system strength including converter control action is challenging as no previous metric exists. However, system strength has three main indicators:

- A stronger system is more stable and therefore will exhibit greater robustness which can be measured using traditional stability techniques.
- A greater strength will provide more damping of oscillations on the network
- A greater strength can provide more reactive support and therefore increased active power flow

Hence, when converter behaviour is included and the GSIM is higher it is expected that the system is more stable,

This article has been accepted for publication in IEEE Transactions on Power Delivery. This is the author's version which has not been fully edited and content may change prior to final publication. Citation information: DOI 10.1109/TPWRD.2022.3233455

oscillations will be better damped and can transfer more power. If GSIM correctly indicates strength considering converters, then the behaviour of the system in terms of the points above containing converters, should be similar to the behaviour of the traditional system with SCR set to the GSIM value obtained when converters are considered. This comparison is made for each indicator in the following section excluding the voltage disturbances as the method used for testing is not applicable to the standalone traditional network model.

A. Stability Analysis

Traditional impedance-based stability methods can be employed to validate the system strength indicated by GSIM. The analysis requires the formulation of transfer functions that describe the current at the PCC using the system provided in Fig. 4. The process for determining the transfer functions is described in [15]. For a single converter connected to the network:

$$\boldsymbol{i}_{pcc} = \frac{\boldsymbol{v}_g \boldsymbol{Y}_{c1}}{\boldsymbol{I}_2 + \boldsymbol{Z}_g \boldsymbol{Y}_{c1}} + \frac{\boldsymbol{i}_{c1} \boldsymbol{I}_2}{\boldsymbol{I}_2 + \boldsymbol{Z}_g \boldsymbol{Y}_{c1}} \tag{39}$$

Where $\boldsymbol{v}_g$ and $\boldsymbol{Z}_g$ are the grid voltage and impedance respectively. $\boldsymbol{i}_{c1}$ and $\boldsymbol{Y}_{c1}$ are the first converter current and admittance, respectively and $\mathbf{I}_2$ is an identity matrix of rank two. When two converters are considered, a different approach becomes more complex. The current at the PCC is determined by first combining the grid in parallel with the first converter of the original system:

$$\boldsymbol{Y}_p = \frac{1}{\boldsymbol{Z}_p} = \boldsymbol{Y}_g + \boldsymbol{Y}_{c1} \tag{40}$$

The current at the PCC is then determined from the Norton equivalent circuit:

$$\boldsymbol{i}_{pcc} = \frac{(\boldsymbol{i}_{c2})}{\boldsymbol{I}_2 + \boldsymbol{Y}_{c2}\boldsymbol{Z}_p} - \frac{(\boldsymbol{i}_{c1})\boldsymbol{Y}_{c2}\boldsymbol{Z}_p}{\boldsymbol{I}_2 + \boldsymbol{Y}_{c2}\boldsymbol{Z}_p} - \frac{(\boldsymbol{i}_g)\boldsymbol{Y}_{c2}\boldsymbol{Z}_p}{\boldsymbol{I}_2 + \boldsymbol{Y}_{c2}\boldsymbol{Z}_p} \tag{41}$$

Where $\boldsymbol{i}_{c2}$ and $\boldsymbol{Y}_{c2}$ are the second converter current and admittance, respectively and $\boldsymbol{i}_g$ is the grid current. The stability of the system is now governed by the more complex transfer function [15]:

$$\frac{\boldsymbol{Y}_{c2}\boldsymbol{Z}_p}{\boldsymbol{I}_2 + \boldsymbol{Y}_{c2}\boldsymbol{Z}_p} \tag{42}$$

The relative stability of each system can be determined by control system margins. Traditional gain and phase margins are not sufficient for complex MIMO systems. Therefore, a robust control analysis technique known as disk margins are employed [36]. Note that there is no direct mathematical relation between the stability margins and GSIM as they analyse different mathematical functions. However, a larger GSIM indicates greater strength and likely a more robust system. Disk margins consider complex perturbations in all loops at once to give a better idea of real stability margins. With disk margins, gain and phase margins are considered as a complex factor f, of the form:

$$f \in D(\alpha, \sigma) = \left\{ \frac{1 + \frac{1-\sigma}{2}\delta}{1 - \frac{1-\sigma}{2}\delta} : \delta \in \mathbb{C}, |\delta| < \alpha \right\} \tag{43}$$

Where the set $D(\alpha, \sigma)$ defines the complex set of perturbations. If the disk skew factor σ, is selected to be 0 the overall perturbation gain can increase or decrease by the same magnitude. The disk margin can then be defined as the maximum value of α that allows fL to remain stable for all $f \in D(\alpha, \sigma)$ where L is the closed loop system gain. The disk margin represents the shortest complex distance from the Nyquist plot of the eigenloci to the critical point. The disk margins are applied to both channels simultaneously for all systems and are shown in Table III.

Table III Comparing GSIM to MIMO Stability Margins

System	GSIM Unscaled	GSIM Scaled	Disk Margin
GFL (y_{sys1})	2.52	1.65	0.42
	6.35	5.61	1.08
GFM (y_{sys2})	8.92	4.42	0.87
	16.7	7.17	1.32
GFL+GFM (y_{sys3})	4.52	1.98	0.86
	8.51	3.4	1.25

From Table III, the system robustness using disk margins follows the strength rating provided by GSIM. Note that a disk margin (< 1) does not carry the same meaning as traditional margins. The gain and phase perturbation related to the disk are still (> 1) and indicate positive stable margins [36]. The largest disk margin of 1.32 occurs for the largest scaled GSIM of 7.17. The ratings of both GSIM and disk margin decrease in the order of y_{sys2}, y_{sys3} to y_{sys1} from strongest to weakest for each SCR. This suggests that the different values of GSIM are correctly replicating the differing behaviour of GFL and GFM in terms of the first indicator of system strength. Conversely, other metrics such as ESCR and CSCR which are equal for both structures suggest the behaviour is the same which does not follow the margins deduced. Moreover, if a traditional network is specified with SCRs equal to the GSIM obtained for y_{sys2} of 4.42 and 7.17, respectively. The disk margins obtained from the PoV of the GFL converter looking into the traditional network are 0.89 and 1.22, respectively. These margins are similar to the margins obtained for y_{sys2}. This suggests that the GFM converter is providing the increased system strength captured by GSIM as the system behaves comparably to a stronger traditional network of the same rating. Note, that for the traditional system the SCR and GSIM are equal offering further justification of the values obtained as the same rating of strength is obtained via GSIM for both the converter based and traditional systems despite the SCR being different. When comparing the scaled and unscaled GSIM versions, the unscaled version appears to overestimate the strength of the network greatly in each case.

B. Voltage Disturbances

The ability of the system to reject voltage disturbances should increase with system strength. To justify the larger GSIM rating for GFM converters, a load of (0.5 + j0.3) MW is suddenly switched into the PCC to disturb the network and the resultant perturbation is studied at three frequencies. The magnitude of voltage disturbance is provided alongside the GSIM at disturbance frequency in Table IV.

From Table IV, the voltage disturbances are larger when the GFL converters operates alone for the respective initial SCRs. The size of the perturbation is similar for y_{sys2} and y_{sys3} despite the large difference in GSIM. However, this is

This article has been accepted for publication in IEEE Transactions on Power Delivery. This is the author's version which has not been fully edited and content may change prior to final publication. Citation information: DOI 10.1109/TPWRD.2022.3233455

due to the different base powers of the system which are specified in (37) and (38) due to one converter being removed in y_{sys2}. Accounting for this, the magnitude of the disturbances is largely in agreement with the rating of GSIM. This method of validation provides certain drawbacks as the introduction of a load may introduce further interactions in the system. However, it is clear that GFM converters reduce the magnitude of voltage perturbations in the network compared to GFL. This indicates a stronger system which is correctly identified by the GSIM.

Table IV Voltage Disturbance Ratios

System	$\lvert\Delta V_i/\Delta V_j\rvert$ (GSIM)		
	75 Hz	125 Hz	175 Hz
GFL	0.403 (1.45)	0.317 (1.58)	0.235 (1.78)
(Y_{sys1})	0.276 (5.55)	0.203 (5.57)	0.178 (5.61)
GFM	0.274 (5.05)	0.208 (5.18)	0.186 (5.21)
(Y_{sys2})	0.187 (6.24)	0.159 (6.29)	0.150 (6.29)
Full	0.247 (2.19)	0.151 (2.27)	0.113 (2.31)
(Y_{sys3})	0.179 (2.91)	0.143 (2.94)	0.128 (2.96)

C. Power Flow

The traditional SCR is often used to infer the active power transfer capabilities of a system. While instabilities caused by interactions between active power flow and voltage are likely not small-signal issues, the impedances determined from small-signals models can be used to infer the power transfer capabilities of the system. The absolute maximum power is determined by the line impedance to the grid as the power capability cannot be violated. However, the connected generation determines how much of this transfer capability can be utilised. GFLs exhibit instabilities when operating close to the physical line limit due to the non-linear relationship between power and voltage [37]. However, GFMs can operate right up to the maximum angle without instability and allow GFLs to increase their maximum angle. The GSIM can represent this feature. New operating points must be utilised for the impedance models that are closer to the limit of power transfer. For y_{sys3}, the active power contribution is considered solely from the GFL converter. This is to allow comparison between the strength provided from the GFM converter and from the traditional network. The converter is assumed to have no current limit to allow high power operation for validation purposes. The GSIM is plotted for the three systems for each SCR in Fig. 6.

From Fig. 6 (a)(b), the GFL converter weakens the network more at higher operating points which can be seen from the lower GSIM rating compared to Fig. 5. This is due to the higher equivalent converter impedance from the increased reactive power contribution to support the PCC. In the case of GFM in Fig. 6 (c)(d), the strengthening of the network is reduced compared to the normal operating point in Fig. 5. However, the converter still contributes increased support to the PCC, allowing higher power operation. When considering the combination of converters in Fig. 6 (e)(f), the GSIM at the FF is higher than when only a single converter is connected. One reason for this is the respective reactive power contribution from each converter is smaller, lowering the effective impedance. The results are compared to time domain simulations where the power output from the respective converter was ramped until the system became unstable. The maximum active power transfer is shown alongside scaled and unscaled GSIMs in Table V.

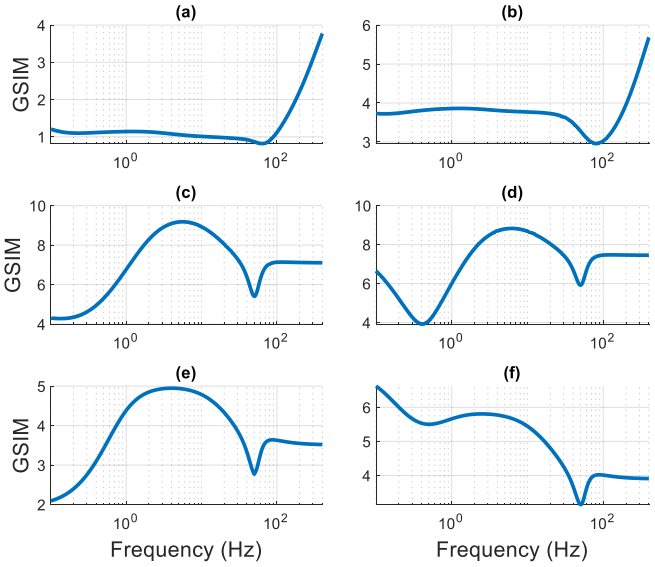

Fig. 6. GSIM at power transfer limit: (a) Y_{sys1} - SCR 1 (b) Y_{sys1} −SCR 3 (c) Y_{sys2} -SCR 1 (d) Y_{sys2} -SCR 3 (e) Y_{sys3} -SCR 1 (f) Y_{sys3} –SCR 3

Table V Problematic Frequency Modes

System	Power Transfer		GSIM (unscaled)	
	SCR 1	SCR 3	SCR 1	SCR 3
Y_{sys1}	3.8 MW	9.8 MW	1.2 (2.5)	3.73 (15.4)
Y_{sys2}	5.7 MW	16.8 MW	4.3 (6.2)	6.64 (14.8)
Y_{sys3}	5.52 MW	15.7 MW	1.82 (9.14)	5.86 (9.0)

From Table V considering SCR 1, the maximum power transfer is worst for the GFL converter. The GFM converter improves this significantly, which is consistent with the GSIMs calculated. The same agreement can be seen between the time domain simulations and the GSIM calculation at an initial SCR 3. Similar to Section IV, the unscaled GSIMs provide an exaggerated view of system strength. If the unscaled values for GFL and GFM are compared for an SCR of 3, the GFL converter appears to provide more strength than the GFM which is incorrect based on the maximum power flows. To further validate the approach, a traditional network with SCR equal to the GSIMs obtained for y_{sys3} is specified. A GFL converter is then connected and the maximum power flow is obtained as 5.74 MW when the SCR is 1.82 and 15.6 MW when the SCR is 5.86. Note, y_{sys3} is used instead of y_{sys2} as with the stability margins, as the power flow must be determined after the connection of the converter. These values are similar to that of y_{sys3} with an error of -4 % and 0.64 %, respectively. This indicates that the GSIM provides a similar rating of strength for a converter dominated network, as the SCR provides for the traditional network in terms of power flow.

VII. Conclusion

This paper has successfully proposed and validated a new method of classifying network strength using system impedances including IBRs. The approach separates system strength from fault current provision, which is necessary in converter dominated systems. Both the useful and detrimental behaviour of different controller structures including GFM and GFL has been represented. This was

achieved by considering the equivalent MIMO converter impedance in the synchronous reference frame. The method has been validated using three main indicators of system strength: improved stability margins, greater voltage disturbance damping and larger active power flow. Each technique indicated that GFM converters increased the system strength which was correctly captured by GSIM. GSIM is applicable to larger networks providing that an impedance trace can be obtained. The wider system can be collapsed into a simpler Thevenin form for analysis similar to previous techniques.

ACKNOWLEDGMENT

Callum Henderson is supported by the Engineering and Physical Sciences Research Council, [EP/R513349/1]. All results can be fully reproduced using the methods and data described in this paper and references provided.

REFERENCES

[1] Department for Business Energy and Industrial Strategy, "Energy Trends UK, April to June 2021," *Statistical Release. September 2021*, 2021.
[2] H. Urdal, R. Ierna, and A. J. Roscoe, "Stability challenges & solutions for power systems operating close to 100% penetration of power electronic interfaced power sources : exchange of experience between hybrid and major power systems," presented at the 3rd International Hybrid Power Systems Workshop, 2018.
[3] NREL, "Technical Report: Understanding Fault Characteristics of Inverter-Based Distributed Energy Resouces," 2010.
[4] N. Nimpitiwan, G. T. Heydt, R. Ayyanar, and S. Suryanarayanan, "Fault Current Contribution From Synchronous Machine and Inverter Based Distributed Generators," *IEEE Transactions on Power Delivery*, vol. 22, no. 1, pp. 634-641, 2007, doi: 10.1109/tpwrd.2006.881440.
[5] C. Henderson *et al.*, "Exploring an Impedance-Based SCR for Accurate Representation of Grid-Forming Converters " presented at the Power Engineering Society General Meeting 2022, Denver, Colorado, USA, 17th - 21st July, 2022.
[6] *IEC TR 60909-4:2021 - Short-circuit current in three-phase AC systems*, B. S. Institution, UK, 2021.
[7] R. Fernades, S. Achilles, and J. MacDowell, "Report to NERC ERSTF for Composite Short Circuit Ratio (CSCR) Estimation Guideline," *GE Energy Consulting*, 2015.
[8] Y. Zhang, S.-H. F. Huang, J. Schmall, J. Conto, J. Billo, and E. Rehman, "Evaluating system strength for large-scale wind plant integration," 2014 2014: IEEE, doi: 10.1109/pesgm.2014.6939043.
[9] CIGRE, "Connection of wind farms to weak AC networks," *Working Group B4.62*, 2016.
[10] J. Jia, G. Yang, A. H. Nielsen, and V. Gevorgian, "Investigation on the Combined Effect of VSC-Based Sources and Synchronous Condensers Under Grid Unbalanced Faults," *IEEE Transactions on Power Delivery*, vol. 34, no. 5, pp. 1898-1908, 2019, doi: 10.1109/tpwrd.2019.2914342.
[11] M. Davari and Y. A.-R. I. Mohamed, "Robust Vector Control of a Very Weak-Grid-Connected Voltage-Source Converter Considering the Phase-Locked Loop Dynamics," *IEEE Transactions on Power Electronics*, vol. 32, no. 2, pp. 977-994, 2017.
[12] I. Ray and L. M. Tolbert, "The Case Against Phase-Locked Loops in Weak AC Grids," 2019 2019: IEEE.
[13] NERC, "Integrating Inverter-Based Resources into Low Short Circuit Strength Systems - Reliability Guideline," 2017.
[14] A. Egea-Alvarez, S. Fekriasl, F. Hassan, and O. Gomis-Bellmunt, "Advanced Vector Control for Voltage Source Converters Connected to Weak Grids," *IEEE Transactions on Power Systems*, vol. 30, no. 6, pp. 3072-3081, 2015, doi: 10.1109/tpwrs.2014.2384596.
[15] C. Henderson, A. Egea-Alvarez, and L. Xu, "Analysis of multi-converter network impedance using MIMO stability criterion for multi-loop systems," *Electric Power Systems Research*, vol. 211, p. 108542, 2022/10/01/ 2022.
[16] G. Wu *et al.*, "Low-Frequency Converter-Driven Oscillations in Weak Grids: Explanation and Damping Improvement," *IEEE Transactions on Power Systems*, vol. 36, no. 6, pp. 5944-5947, 2021.
[17] C. Henderson, D. Vozikis, D. Holliday, X. Bian, and A. Egea-Àlvarez, "Assessment of Grid-Connected Wind Turbines with an Inertia Response by Considering Internal Dynamics," *Energies*, vol. 13, no. 5, 2020, doi: 10.3390/en13051038.
[18] A. Abdelrahim, M. Smailes, K. H. Ahmed, P. McKeever, and A. Egea-Alvarez, "New Fault Detection Algorithm for an Improved Dual VSM Control Structure With FRT Capability," *IEEE Access*, vol. 9, pp. 125134-125150, 2021, doi: 10.1109/access.2021.3109165.
[19] A. Tuckey and S. Round, "Practical application of a complete virtual synchronous generator control method for microgrid and grid-edge applications," 2018 2018: IEEE.
[20] Q.-C. Zhong and G. Weiss, "Synchronverters: Inverters That Mimic Synchronous Generators," *IEEE Transactions on Industrial Electronics*, vol. 58, no. 4, pp. 1259-1267, 2011, doi: 10.1109/tie.2010.2048839.
[21] A. Abdelrahim, P. Mckeever, M. Smailes, A. Egea-Àlvarez, and K. H. Ahmed, "Modified grid forming converter controller with fault ride through capability without PLL or current loop," 2019.
[22] X. Yue, X. Wang, and F. Blaabjerg, "Review of Small-Signal Modeling Methods Including Frequency-Coupling Dynamics of Power Converters," *IEEE Transactions on Power Electronics*, vol. 34, no. 4, pp. 3313-3328, 2019, doi: 10.1109/tpel.2018.2848980.
[23] Z. Haoxiang, L. Jing, Z. Chen, C. Xu, M. Molinas, and R. Fangquan, "Mimo impedance based stability analysis of DFIG-based wind farm with MMC-HVDC in modifed sequence domain," 2019 2019: Institution of Engineering and Technology.
[24] Q. Xiao, P. Mattavelli, A. Khodamoradi, and F. Tang, "Analysis of transforming dq impedances of different converters to a common reference frame in complex converter networks," *CES Transactions on Electrical Machines and Systems*, vol. 3, no. 4, pp. 342-350, 2019.
[25] W. Zhou, R. E. Torres‐Olguin, Y. Wang, and Z. Chen, "DQ impedance‐decoupled network model‐based stability analysis of offshore wind power plant under weak grid conditions," *IET Power Electronics*, vol. 13, no. 13, pp. 2715-2729, 2020, doi: 10.1049/iet-pel.2019.1575.
[26] C. Li, J. Liang, L. M. Cipcigan, W. Ming, F. Colas, and X. Guillaud, "DQ Impedance Stability Analysis for the Power-Controlled Grid-Connected Inverter," *IEEE Transactions on Energy Conversion*, vol. 35, no. 4, pp. 1762-1771, 2020, doi: 10.1109/tec.2020.2989855.
[27] A. Rygg, M. Molinas, E. Unamuno, C. Zhang, and X. Cai, "A simple method for shifting local dq impedance models to a global reference frame for stability analysis," *arXiv pre-print server*, 2017-06-26 2017.
[28] J. Khazaei, Z. Miao, and L. Piyasinghe, "Impedance-model-based MIMO analysis of power synchronization control," *Electric Power Systems Research*, vol. 154, pp. 341-351, 2018.
[29] E. Unamuno, A. Rygg, M. Amin, M. Molinas, and J. A. Barrena, "Impedance-Based Stability Evaluation of Virtual Synchronous Machine Implementations in Converter Controllers," 2018 2018: IEEE.
[30] A. Bolzoni, "Generalized Nyquist MIMO Stability of Frequency Regulation Services in Power Networks," 2020 2020: IEEE.
[31] Y. Wang, X. Wang, F. Blaabjerg, and Z. Chen, "Frequency scanning-based stability analysis method for grid-connected inverter system," 2017 2017: IEEE.
[32] R. N. Damas, Y. Son, M. Yoon, S.-Y. Kim, and S. Choi, "Subsynchronous Oscillation and Advanced Analysis: A Review," *IEEE Access*, vol. 8, pp. 224020-224032, 2020.
[33] L. Harnefors, "Analysis of Subsynchronous Torsional Interaction With Power Electronic Converters," *IEEE Transactions on Power Systems*, vol. 22, no. 1, pp. 305-313, 2007, doi: 10.1109/tpwrs.2006.889038.
[34] S. Ghosh, K. V. Kkuni, G. Yang, and L. Kocewiak, "Impedance scan and characterization of Type 4 wind power plants through aggregated model," 2019 2019: IEEE.
[35] A. Rygg, M. Molinas, C. Zhang, and X. Cai, "A Modified Sequence-Domain Impedance Definition and Its Equivalence to the dq-Domain Impedance Definition for the Stability Analysis of AC Power Electronic Systems," *IEEE Journal of Emerging and Selected Topics in Power Electronics*, vol. 4, no. 4, pp. 1383-1396, 2016.
[36] P. Seiler, A. Packard, and P. A. Gahinet, "An Introduction to Disk Margins," *IEEE Control Systems Magazine*, 2020.
[37] C. Henderson, N. McNeill, G. Wu, D. Holliday, and A. Egea-Àlvarez, "Vector Control of a Single-Phase Voltage Source Converter For the Supply of Inertia to Weak Grids," 2021 2020: Institution of Engineering and Technology.